Journal of Hazardous Materials 197 (2011) 272–284

Contents lists available at SciVerse ScienceDirect

Journal of Hazardous Materials

journal homepage: www.elsevier.com/locate/jhazmat

Low frequency US and UV-A assisted Fenton oxidation of simulated dyehouse wastewater

Ivana Grčić, Marija Maljković, Sanja Papić*, Natalija Koprivanac

Department of Polymer Engineering and Organic Chemical Technology, Faculty of Chemical Engineering and Technology, University of Zagreb, Marulićev trg 19, HR-10000 Zagreb, Croatia

ARTICLE INFO

Article history:
Received 27 May 2011
Received in revised form
15 September 2011
Accepted 22 September 2011
Available online 29 September 2011

Keywords:
Simulated dyehouse wastewater
US and UV-A Fenton process
Box–Behnken design
Mixture design
Optimization
Surfactants

ABSTRACT

The scope of the present study was to explore the treatment possibilities for the simulated dyehouse wastewater (WW) by the Fenton oxidation ultrasonic (US) or UV-A assisted. Composition of WW included reactive azo dye, C.I. Reactive Violet 2 (RV2), anionic surfactant (LAS) and auxiliary chemicals. An emphasis was put on the influence of the LAS on the treatment efficiency. To explore the pseudo-catalytic effect of LAS and reagent dosages on the extents of decolourization and mineralization, different experimental design techniques were utilized. Box–Behnken design was used as a base for optimization and determination of the influencing factors; numerical ($Fe^{2+/3+}$, H_2O_2 and LAS concentration) and categorical factors (iron oxidation state and type of additional energy; US or UV-A). Furthermore, a mixture design methodology was applied. This *two-step* optimization approach lead to a single optimal point for two advanced oxidation processes studied in comparison. Models describing the dependency of the overall efficiency on influencing factors were obtained. Application of US/Fe^{2+}/H_2O_2 and UV-A/Fe^{2+}/H_2O_2 processes for the treatment of WW was assessed. Only 26% of mineralization was achieved by Fenton process alone applied for the treatment of the dyehouse effluent in 10-fold dilution, while 43% of mineralization was achieved by US or UV-A assisted Fenton after the 60 min.

1. Introduction

The textile industry is considered to be a worldwide water-pollution source [1]. Effluents arising from dyeing facilities and finishing operations in textile industries are usually loaded with significant quantities of dyes, causing the colouration of waste streams visible even in concentrations such as 1 mg L^{-1}. Beside the organic dyes, an elevated concentration of the detergents and other additional dyeing reagents could be found in the dye bath effluents. Hence, a small amount of such effluents discharged into water recipients might significantly change the colour of rivers or lakes inhibiting the transmission of natural light and consequently present a hazard to aquatic ecosystems together with the increase of loading of organic content [2]. Moreover, many synthetic dyes and their degradation by-products present a treat to the ecosystems due to the whole range of hazardous properties [3]. Among all dyes produced today a group of reactive dyes participates with a large portion and becomes the most remarkable due to specific characteristics of linkage between colourant and natural fibers. Due to high stability, solubility in water and low biodegradability of azo dyes it is necessary to find an effective method for the treatment of such effluents. Advanced oxidation processes (AOPs) have been already described as a promising alternative in the removal of the persistent pollutants whereas conventional treatment methods are not efficient enough [4]. In that sense, Fenton reagent, a mixture of Fe salts and H_2O_2, is an attractive oxidative system owing to the simple production of •OH radicals, Eq. (1) [1].

$$Fe^{2+} + H_2O_2 \rightarrow Fe^{3+} + {}^{\bullet}OH + OH^- \quad (1)$$

Although Fenton oxidation is widely accepted as efficient and environmental friendly process, the generation of sludge due to the flocculation of organic Fe(III) complexes and Fe(III) hydroxides at elevated pH values presents its disadvantage. Introduction of ultrasound or ultraviolet irradiation in the systems lead to the enhancement of the Fenton oxidation, Eqs. (2)–(5). Such processes are known as sono-Fenton and photo-Fenton process [2,3,5,6].

$$Fe^{3+} + H_2O \rightarrow [Fe(OH)]^{2+} + H^+ \quad (2)$$

$$[Fe(OH)]^{2+} \xrightarrow[\text{or })))]{h\nu} Fe^{2+} + {}^{\bullet}OH \quad (3)$$

$$Fe^{3+} + H_2O_2 \rightarrow Fe(OOH)^{2+} + H^+ \quad (4)$$

$$Fe(OOH)^{2+} \xrightarrow{)))} Fe^{2+} + HO_2{}^{\bullet} \quad (5)$$

* Corresponding author. Tel.: +385 1 4597 122; fax: +385 1 4597 142.
E-mail addresses: spapic@marie.fkit.hr, spapic@fkit.hr (S. Papić).

0304-3894/$ – see front matter © 2011 Elsevier B.V. All rights reserved.
doi:10.1016/j.jhazmat.2011.09.084

Table 1
Chemical composition and characteristics of the simulated dyehouse effluent.

Dyestuff	Manufacturer			Concentration ($mg\,L^{-1}$)
C.I. Reactive Violet 2	CIBA			100
Auxiliary chemical	**Manufacturer**	**Function**	**Commercial name**	**Concentration ($g\,L^{-1}$)**
Sodium salt of dodecylbenzene sulfonic acid (LAS)	Aldrich	Detergent used for washing out the excess dye	–	1
Polyether based co-polymer	CHT Tübingen (UK)	Anti-creasing agent	DENIMCOL RT	0.6
Phosphorous free acryl co-polymer mixture	Textilcolor (Germany)	Sequestering agent	ALVIROL AGK	0.4
NaOH	Kemika (Croatia)	Forms covalent bonds between dye and fabric	–	0.51
NaCl		Electrolyte used for aggregation of dye onto fabric	–	41
Na_2CO_3		pH buffer	–	13
Glacial acetic acid	Alkaloid (Macedonia)	Neutralization	–	0.79
TOC value of the mixture ($mg\,L^{-1}$)				1769
pH value of the mixture				10.0

The continuous reduction of Fe^{3+} to Fe^{2+} shown above allows the oxidation to start again, Eq. (1), using the regenerated Fe^{2+}. Moreover, irradiation contributes to decrease in the sludge production. Consequently, Fe^{2+} can be generated from the organic Fe(III) complexes, Fe^{3+}–OC, Eq. (6) [7].

$$Fe^{3+}\text{–OC} + h\nu \rightarrow Fe^{2+} + \text{organic radical} \quad (6)$$

Recently, the similar effect has been observed when ultrasound was employed [8]. On the other hand, application of ultrasound has been an issue of numerous investigations due to the acoustic cavitation and related phenomena [9]. The collapse of the cavitation bubbles generated by ultrasound field (sonication) leads to formation of hotspots with extremely high local conditions of temperature and pressure, which allow the formation of reactive radicals, such as $H^{\bullet}$, $^{\bullet}OH$, $O_2^{\bullet -}$, as well as the homolytic splitting of polluted compounds [5]. The degradation of organic compounds in aqueous sonicated system takes place at three potential reaction sites; (i) inside of the cavitation bubble, (ii) the gas–liquid interfacial region (bubble surface), and (iii) in the bulk solution (surrounding liquid) [10]. Two main reaction mechanisms are proposed; (i) oxidation by OH radicals at all reaction sites, and (ii) thermolysis inside cavitation bubbles and at the bubble surface [11,12].

Sonochemical oxidation of surfactants is expected to be rather effective since surfactants preferentially accumulate and react at cavitation bubble surfaces. Furthermore, surfactants left in the bulk solution react with the $^{\bullet}OH$ radicals diffusing from bubble surfaces [11].

The aim of this paper was to explore the possibility of the treatment of simulated dyehouse wastewater by US and UV-A assisted Fenton process, US/Fe^{2+}/H_2O_2 and UV-A/Fe^{2+}/H_2O_2, respectively. The specific objectives included studying the influence of the surfactant on decolourization and mineralization of dye solution and optimization of the selected processes. Mineralization kinetics has been studied and discussed, including all the effects of the auxiliary chemicals constituting the dye bath effluent.

2. Experimental

2.1. Model solutions

A commercial reactive copper binding monoazo dye, C.I. Reactive Violet 2 (RV2), composed of one monochlorotriazine reactive group, was supplied by Ciba and used as received without any purification. Suppliers for sodium salt of dodecylbenzene sulfonic acid (hereafter: Na-dodecylbenzene sulfonate or LAS) and the other dye assisting chemicals are summarized in Table 1.

The simulated dyehouse effluent (WW) was prepared according to the information that usually 20% of the dyestuff and 100% of all applied dye assisting chemicals remain in the exhausted dyebath [13]. The concentration of the dyebath consisting chemicals in the simulated dyehouse effluent and the corresponding function of each compound during the dyeing process are summarized in Table 1.

The recipe mixture was treated for 30–60 min, depending on the applied process, in (i) a 10-fold dilution (WW 1:10) corresponding to the typical dyehouse effluent concentration from the washing and rinsing stages of the textile factory [13] or (ii) as prepared (WW).

Nevertheless, model solutions of only $100\,mg\,L^{-1}$ of RV2 or $100\,mg\,L^{-1}$ of RV2 with 50 or $100\,mg\,L^{-1}$ of LAS (RV2+LAS) were used in the experiments performed within the experimental plan used for model development and optimization (Tables 2 and 4).

Concentration of LAS in WW 1:10 correspond to the highest LAS concentration in model solution (RV2+LAS). That particular amount of LAS ($100\,mg\,L^{-1}$ or $0.3 \times 10^{-3}\,mol\,L^{-1}$) was further set as optimization criteria as given in the following subsections.

2.2. Reagents

Sulfuric acid (H_2SO_4, 50%, Kemika, Zagreb, Croatia) was used for the pH adjustment. Reagents for the Fenton type reactions were as follows; ferrous sulfate ($FeSO_4{\cdot}7H_2O$), ferric sulfate ($Fe_2(SO_4)_3{\cdot}9H_2O$) and hydrogen peroxide (H_2O_2 30%), all supplied by Kemika.

2.3. Reactors

The reactor used for the experiments involving the sonication was presented in our previous paper [6]. It is consisted of a borosilicate glass cylindrical batch reactor with the cooling jacket and

Table 2
Control factors and their levels used for the Box–Behnken experimental plan (BBD).

Factor	Code	Levels		
Numerical		(−1)	(0)	(1)
$[Fe] \times 10^3$, $mol\,L^{-1}$	X_1	0.01	1	2
$[H_2O_2]$, $mol\,L^{-1}$	X_2	0	0.03	0.06
γ(LAS), $mg\,L^{-1}$	X_3	0	50	100
Categorical		(1)	(2)	
Type of iron	X_4	Fe^{2+}	Fe^{3+}	
Auxiliary energy	X_5	US	UV	

Table 3
BBD matrix and responses at different factor levels.

Factors						Responses		Transformed responses	
Run number	X_1, $[Fe^{2+/3+}]$, $\times 10^3$, mol L^{-1}	X_2, $[H_2O_2]$, mol L^{-1}	X_3, γ(LAS), mg L^{-1}	X_4, iron ion oxidation state	X_5, auxiliary energy	X_{colour}, %	X_{TOC}, %	$Y_{E,colour}$	$Y_{E,TOC}$
1	1.00	0.06	100.00	II	US	99.90	21.27	4.467	−0.423
2	1.00	0.06	0.00	II	UV-A	99.81	49.14	4.388	2.477
3	1.00	0.00	100.00	III	US	21.32	39.73	−1.529	1.071
4	2.00	0.00	50.00	III	US	20.37	20.27	−1.597	−0.502
5	1.00	0.03	50.00	III	US	100	27.92	4.564	0.086
6	2.00	0.03	100.00	III	UV-A	99.81	18.5	4.388	−0.648
7	1.00	0.00	100.00	II	UV-A	23.85	29.31	−1.360	0.192
8	1.00	0.03	50.00	II	UV-A	98.81	35.31	3.767	0.669
9	1.00	0.00	0.00	II	US	22.51	1.65	−1.447	−3.658
10	1.00	0.06	0.00	III	US	98.05	13.37	3.461	−1.117
11	2.00	0.00	50.00	II	UV-A	43.65	23.12	−0.370	−0.278
12	0.01	0.03	100.00	II	UV-A	7.95	17.59	−3.172	−0.725
13	1.00	0.03	50.00	III	UV-A	99.29	2.00	4.020	−3.418
14	1.00	0.03	50.00	III	US	99.86	5.75	4.431	−2.169
15	0.01	0.03	0.00	II	UV-A	72.58	1.38	0.880	−3.890
16	0.01	0.03	100.00	II	US	7.47	17.86	−3.309	−0.702
17	1.00	0.03	50.00	II	UV-A	98.48	34.09	3.624	0.567
18	0.01	0.00	50.00	II	UV-A	9.14	1.32	−2.893	−3.950
19	2.00	0.06	50.00	II	US	100	3.49	4.564	−2.753
20	1.00	0.00	0.00	II	UV-A	43.65	5.16	−0.370	−2.296
21	1.00	0.03	50.00	II	UV-A	98.70	27.09	3.717	0.023
22	2.00	0.03	0.00	II	US	100	29.40	4.564	0.199
23	1.00	0.00	0.00	II	UV-A	33.16	33.67	−0.846	0.533
24	0.01	0.06	50.00	III	UV-A	17.23	24.27	−1.849	−0.190
25	1.00	0.00	100.00	II	US	24.65	30.55	−1.310	0.287
26	0.01	0.03	100.00	III	UV-A	5.27	5.94	−4.363	−2.130
27	1.00	0.03	50.00	III	UV-A	99.62	11.85	4.238	−1.278
28	1.00	0.03	50.00	III	US	100	6.01	4.564	−2.116
29	0.01	0.06	50.00	II	UV-A	46.79	3.70	−0.238	−2.685
30	2.00	0.03	100.00	II	US	99.90	5.26	4.467	−2.273
31	1.00	0.03	50.00	III	UV-A	99.86	25.00	4.431	−0.135
32	0.01	0.06	50.00	III	US	41.41	6.33	−0.467	−2.055
33	2.00	0.03	100.00	III	US	100	5.85	4.564	−2.148
34	1.00	0.03	50.00	II	US	99.73	23.40	4.322	−0.257
35	0.01	0.03	0.00	II	US	64.45	16.23	0.502	−0.844
36	0.01	0.03	0.00	II	UV-A	84.53	7.57	1.586	−1.840
37	1.00	0.03	50.00	II	UV-A	99.50	28.40	4.153	0.123
38	1.00	0.03	50.00	III	UV-A	99.29	4.30	4.020	−2.509
39	2.00	0.00	50.00	III	UV-A	25.37	22.79	−1.266	−0.304
40	1.00	0.06	100.00	III	UV-A	100	13.80	4.564	−1.074
41	2.00	0.03	0.00	III	UV-A	99.86	37.43	4.431	0.853
42	0.01	0.00	50.00	III	UV-A	12.80	18.50	−2.311	−0.648
43	1.00	0.03	50.00	II	UV-A	99.95	45.78	4.515	1.807
44	1.00	0.06	100.00	III	US	100	4.17	4.564	−2.545
45	0.01	0.03	0.00	III	US	58.97	1.64	0.267	−3.666
46	1.00	0.06	0.00	II	US	99.52	17.52	4.167	−0.731
47	2.00	0.06	50.00	III	UV-A	100	21.18	4.564	−0.430
48	1.00	0.03	50.00	II	US	97.24	10.15	3.210	−1.478
49	2.00	0.03	0.00	II	UV-A	99.14	52.24	3.934	3.950
50	1.00	0.06	0.00	III	UV-A	99.48	41.19	4.140	1.221
51	0.01	0.00	50.00	II	US	11.47	11.71	−2.490	−1.294
52	1.00	0.03	50.00	II	US	99.29	14.81	4.020	−0.975
53	0.01	0.00	50.00	III	US	5.05	15.10	−4.564	−0.948
54	2.00	0.03	0.00	III	US	99.52	22.18	4.167	−0.351
55	2.00	0.06	50.00	III	US	99.81	7.58	4.388	−1.839
56	1.00	0.03	50.00	II	US	98.81	9.82	3.767	−1.520
57	1.00	0.03	50.00	III	US	99.62	18.96	4.238	−0.609
58	2.00	0.06	50.00	II	UV-A	100	26.44	4.564	−0.026
59	1.00	0.00	100.00	III	UV-A	23.13	34.79	−1.406	0.625
60	1.00	0.03	50.00	III	UV-A	99.00	18.00	3.860	−0.690
61	0.01	0.06	50.00	II	US	21.51	27.53	−1.516	0.057
62	0.01	0.03	100.00	III	UV-A	5.27	16.86	−4.363	−0.788
63	1.00	0.03	50.00	II	UV-A	99.52	36.14	4.167	0.739
64	2.00	0.03	100.00	II	UV-A	99.76	12.80	4.346	−1.176
65	1.00	0.00	0.00	III	US	19.22	33.37	−1.685	0.509
66	2.00	0.00	50.00	II	US	29.75	15.37	−1.020	−0.923
67	1.00	0.03	50.00	III	US	99.40	14.00	4.088	−1.054
68	1.00	0.06	100.00	II	UV-A	99.57	10.32	4.202	−1.457

Table 4
Mixture composition at each point of the mixture D-optimal experimental design.

Run number[a]	X_1 [Fe^{2+}] × 10^3, mol L^{-1}	X_2 [H_2O_2], mol L^{-1}	X_3 [LAS] × 10^3, mol L^{-1} [b]
1	0.98	0.05	0.27
2	1.04	**0.06**[c]	**0.20**
3	1.04	0.06	0.20
4	1.03	0.04	0.23
5	**0.95**	0.05	**0.30**
6	1.00	0.06	0.25
7	0.98	**0.02**	0.30
8	0.99	0.03	0.28
9	**1.05**	0.02	0.23
10	0.98	0.02	0.30
11	1.02	0.02	0.27
12	1.05	0.03	0.22
13	1.05	0.02	0.23
14	0.95	0.05	0.30

[a] Each run was simulated using the relevant model equations (as a result of BBD).
[b] M(LAS) = 348.48 g mol^{-1}.
[c] Bold values indicate the concentration range for each mixture compound.

the maximum working volume of 0.75 L and an immersed ultrasonic horn placed vertically in the middle of the reactor (ultrasonic homogenizer SONOPLUS HD 2200, Bandelin, Germany) operating at 20 kHz. The amplitude in the performed experiments was adjusted at 100% continuously, without pulse length setup, resulting with the power efficiency of 27.9% (0.5 L working volume) at 20 kHz and 200 W input condition [6].

The experiment involving the employment of UV-A light was performed in a borosilicate glass cylindrical batch photo reactor of 0.8 L total volume, with sampling ports on the top, magnetic stirrer and water jacket for temperature control [14]. The irradiation source was low pressure mercury UV lamp (PenRay 90-0019-04, UV-A 365 nm, UVP-Ultra Violet Products, Cambridge, UK) with typical intensity of 1.255 W cm^{-2} (λ = 365 nm) at 2 cm distance of the source. UV lamp was placed axially in a quartz tube inside the reactor.

The temperature in the both reactors was monitored during the sonication time and kept constant, 29 ± 3 °C. Temperature and pH of the system were continuously monitored by pH/conductivity meter with the integrated NTC 30/Pt1000 temperature sensor (Handylab LF 12, Schott, Germany.

Experiments without sonication or irradiation were performed as jar-tests in glass reaction vessels with the maximum reaction volume of 0.6 L and constant magnetic stirring (450 rpm) in a thermostated bath, 29 ± 2 °C placed in a silent dark chamber.

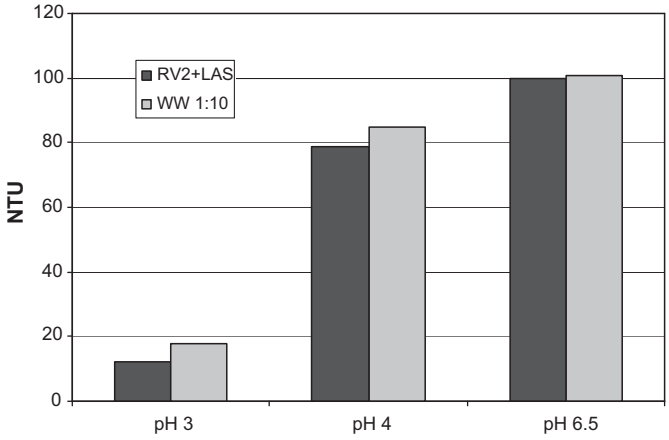

Fig. 1. Measured turbidity in WW and RV2+LAS solution (t = 0 min) at different pH values.

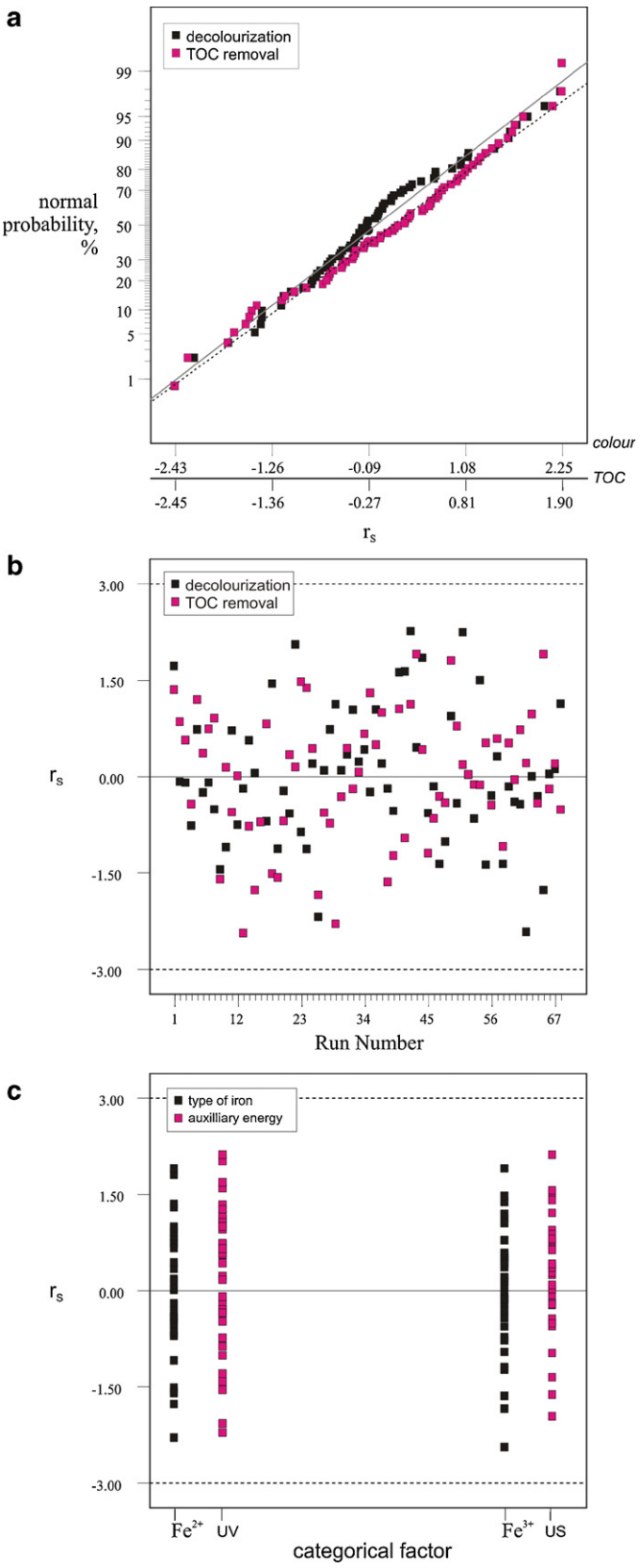

Fig. 2. Validation of statistical models for US/UV-A Fenton type processes (RV2+LAS solution); (a) normal probability plots, (b) and (c) residuals plots (r_S).

2.4. Chemical assays and characterization

Mineralization extents were determined on the basis of total organic carbon content measurements (TOC), performed by using total organic carbon analyzer; TOC-V_{CPN} 5000 A, Shimadzu. A Perkin–Elmer Lambda EZ 201 UV/VIS spectrophotometer was used for dye degradation monitoring in the wavelength range from 200 to 700 nm. Turbidity was measured by Hach 2100P Turbidimeter (USA).

2.5. Experimental design

In the first step, a response surface three-level spherical Box–Behnken design (BBD), commonly chosen for the purpose of response optimization [15,16], was used as a base for the experimental data analysis, model development and optimization through a desirability function approach (DFA) – *first step*. BBD with three numeric factors, varied over three levels (Table 2) was used to determine the operating conditions for maximizing the organic content reduction, i.e. mineralization extent and decolourization yield (dye degradation). Since two additional categorical factors, at two levels (Table 2), were involved, design was duplicated for each combination of the categorical factor levels, resulting in total of 68 experiments conducted under the conditions defined in Table 3, in random manner.

In the second step, the D-optimal mixture design was used to find a single optimal point within the area given by DFA based on BBD models. The main characteristic of a mixture design is that the single components cannot be changed independently of one another since their sum must add up to 1 (or 100%). This means that mixture components/factors are expressed as the fraction of the total amount and their experimental ranges lie between 0 and 1 [17]. Since the given area represents an irregular experimental region, D-optimal design was used to ensure the well-handling with the irregularity since it provides the best simultaneous estimate of the model parameters or mixture components [18–20]. The resulting experimental design is shown in Table 4. Responses were then simulated from the BBD models, and the another set of auxiliary models were developed (Table 6). DFA was applied again to establish the final optimal composition of the mixture.

The *Design-Expert 6.0.6* software package (Stat-Ease, Inc.) was used.

3. Results and discussion

3.1. Experimental design and optimization

Both ultrasonic and photo assisted Fenton oxidation have been thoroughly studied, and a *two-step* optimization has been performed. However, initial pH value in the treated system was kept constant (pH 3) due to the high turbidity of the system measured at higher pH values (Fig. 1). Higher turbidity in the system could result with the negative impact on the overall efficiency achieved by the UV-A assisted process. Presence of the suspended solids contributes to the erratic light scattering and decrease in the observed quantum yield. In the case of ultrasonic assisted process, suspended solids could also have a negative impact on overall efficiency in terms of wave propagation and increase of the cavitational threshold.

As a results of experimental design (BBD) and a consequent analysis, models describing the dependency of the decolourization and mineralization yields on the reagents' dosage ($Fe^{2+/3+}$, H_2O_2) and LAS present in the treated system in case of US and UV-A employment were obtained (Table 6). For current study, response surface models were evaluated using ANOVA. Statistics summary

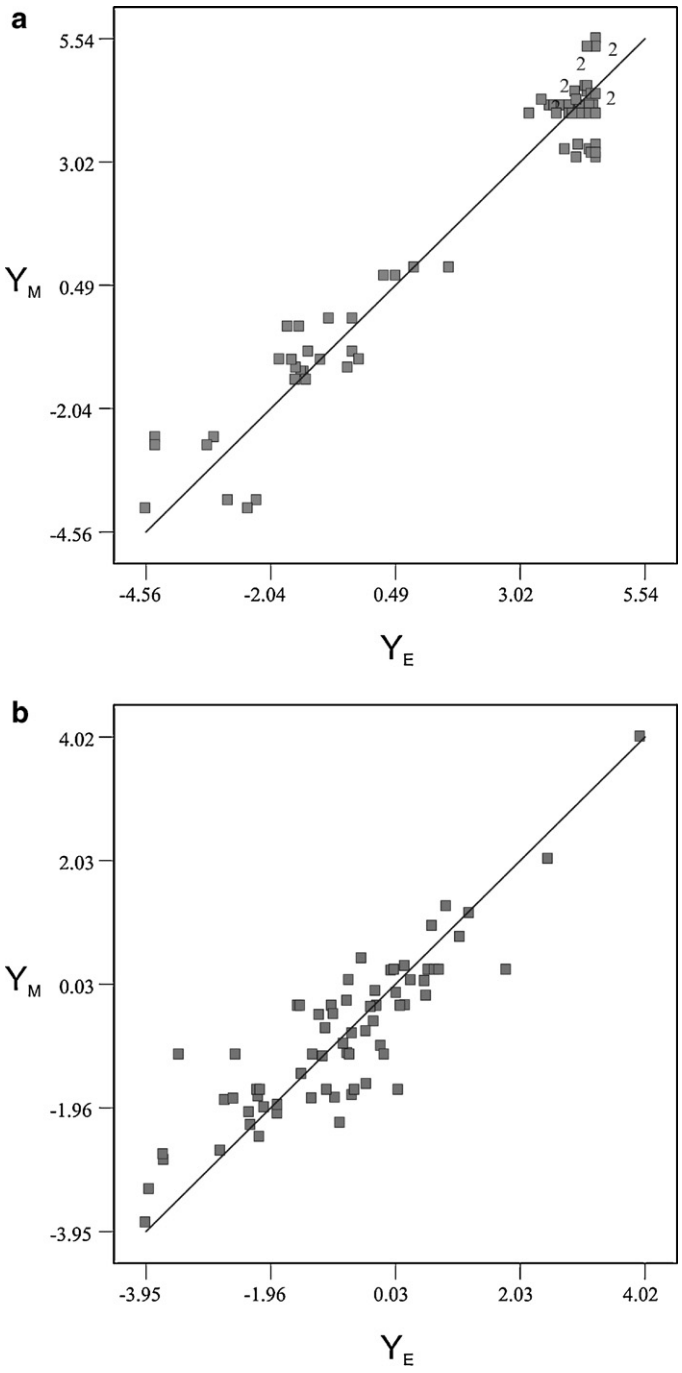

Fig. 3. Predicted vs. actual plots for the transformed responses referred to the (a) decolourization and (b) mineralization achieved by US/UV-A Fenton type processes (RV2+LAS solution). *Note:* number "2" represent the overlapping points.

was given in Table 5. Model *F*-values of 99.59 and 4.30 and *p*-values less than 0.05 imply that the models are significant. Significant terms in each predictive model, with the *p*-value less than 0.05 are given as well (Table 5). Lack of fit is not significant ($p > 0.05$). The obtained models showed a satisfying accuracy and adequacy over the selected design space. Residual analysis gave the structureless residuals (r_S) with no evidence of non-normality (Fig. 2a). The residuals are also equally distributed in the terms of experimental run and studied categorical factors (Fig. 2b and c). Experimental values follow the predicted trend (Fig. 3a and b).

The presented model equations showed the strong dependency of a mineralization rate on the Fenton reagent dosage and LAS

Table 5
Statistics summary for the BBD resulting models.

Model response	X_{colour}, %	X_{TOC}, %
Transformation	*Logit* function	*Logit* function
Lower bound (l.b.)	4.05	0.32
Upper bound (u.b.)	101	53.24
Model	Reduced surface quadratic	Reduced surface 2FI
Significant model terms ($p < 0.05$)	$X_1, X_2, X_3, X_1^2, X_2^2, X_3^2, X_1X_2, X_1X_3$	$X_1, X_5, X_1X_3, X_1X_5, X_2X_3, X_2X_4$
LOF[a] p-value	0.1080	0.1377
Model p-value	<0.0001	<0.0001
Model F-value	99.59	4.30
R^2	0.9392	0.7639
Adjusted R^2	0.9298	0.5273
Predicted R^2	0.9099	0.4840

[a] LOF – lack of fit.

Table 6
Model equations given as a result of response surface BBD and mixture D-optimal design.

Transformed model response	Model equation
Response surface BBD	
$Y_{M,colour}$ (US assisted Fenton)	$-2.8960 + 4.7054[Fe] + 0.1869[H_2O_2] - 0.0150\gamma(LAS) - 2.1774[Fe]^2 - 2.3 \times 10^{-3}[H_2O_2]^2 - 2 \times 10^{-4}\gamma(LAS)^2 + 0.0296[Fe][H_2O_2] + 0.0240[Fe]\gamma(LAS)$
$Y_{M,colour}$ (UV-A assisted Fenton)	$-2.7285 + 4.7054[Fe] + 0.1869[H_2O_2] - 0.0150\gamma(LAS) - 2.1774[Fe]^2 - 2.3 \times 10^{-3}[H_2O_2]^2 - 2 \times 10^{-4}\gamma(LAS)^2 + 0.0296[Fe][H_2O_2] + 0.0240[Fe]\gamma(LAS)$
$Y_{M,TOC}$ (US, Fe^{2+})	$-3.4857 + 1.4314[Fe^{2+}] + 0.0436[H_2O_2] + 0.0402\gamma(LAS) - 0.0105[Fe^{2+}][H_2O_2] - 0.0211[Fe^{2+}]\gamma(LAS) - 6 \times 10^{-4}[H_2O_2]\gamma(LAS)$
$Y_{M,TOC}$ (US, Fe^{3+})	$-2.8127 + 1.4314[Fe^{3+}] + 0.0129[H_2O_2] + 0.0402\gamma(LAS) - 0.0105[Fe^{3+}][H_2O_2] - 0.0211[Fe^{3+}]\gamma(LAS) - 6 \times 10^{-4}[H_2O_2]\gamma(LAS)$
$Y_{M,TOC}$ (UV-A, Fe^{2+})	$-4.0195 + 2.4155[Fe^{2+}] + 0.0642[H_2O_2] + 0.0317\gamma(LAS) - 0.0105[Fe^{2+}][H_2O_2] - 0.0211[Fe^{2+}]\gamma(LAS) - 6 \times 10^{-4}[H_2O_2]\gamma(LAS)$
$Y_{M,TOC}$ (UV-A, Fe^{3+})	$-3.3651 + 2.4155[Fe^{3+}] + 0.0642[H_2O_2] + 0.0317\gamma(LAS) - 0.0105[Fe^{3+}][H_2O_2] - 0.0211[Fe^{3+}]\gamma(LAS) - 6 \times 10^{-4}[H_2O_2]\,\gamma(LAS)$
Mixture D-optimal	
US/Fe^{2+}/H_2O_2	
$X_{colour} \times 10^3$, %	$342[Fe^{2+}\ (mol\,L^{-1})] - 0.385[H_2O_2\ (mol\,L^{-1})] - 16420[LAS\ (mol\,L^{-1})] + 0.463[Fe^{2+}][H_2O_2] + 22361[Fe^{2+}][LAS] + 0.448[H_2O_2][LAS] - 0.236[Fe^{2+}][H_2O_2][LAS] - 0.130[Fe^{2+}][H_2O_2]([Fe^{2+}] - 0.001[H_2O_2]) - 9984[Fe^{2+}][LAS]([Fe^{2+}] - [LAS]) + 0.108[H_2O_2][LAS](0.001[H_2O_2 - [LAS])$
$X_{TOC} \times 10^3$, %	$-956[Fe^{2+}\ (mol\,L^{-1})] - 0.332[H_2O_2\ (mol\,L^{-1})] + 65422[LAS\ (mol\,L^{-1})] + 0.427[Fe^{2+}][H_2O_2] - 89222[Fe^{2+}][LAS] + 0.101[H_2O_2][LAS] - 0.134[Fe^{2+}][H_2O_2]([Fe^{2+}] - 0.001[H_2O_2]) + 38607[Fe^{2+}][LAS]([Fe^{2+}] - [LAS]) - 0.049[H_2O_2][LAS](0.001[H_2O_2 - [LAS])$
UV-A/Fe^{2+}/H_2O_2	
$X_{colour} \times 10^3$, %	$42[Fe^{2+}\ (mol\,L^{-1})] - 36[H_2O_2\ (mol\,L^{-1})] - 185[LAS\ (mol\,L^{-1})] + 30[Fe^{2+}][H_2O_2] + 151[Fe^{2+}][LAS] + 30[H_2O_2][LAS]$
$X_{TOC} \times 10^3$, %	$13[Fe^{2+}\ (mol\,L^{-1})] - [H_2O_2\ (mol\,L^{-1})] + 73[LAS\ (mol\,L^{-1})] + [Fe^{2+}][H_2O_2] - 29[Fe^{2+}][LAS] - 0.4[H_2O_2][LAS]$

Table 7
Optimization criteria and results.

Goal	Criteria	Result	Desirability
Using the BBD and corresponding model equations			
$X_{colour}, X_{TOC} \Rightarrow$ maximum	$[Fe] \rightarrow 1.005 \times 10^{-3}$ mol L^{-1} $[H_2O_2]$ is in range $\gamma(LAS) \rightarrow 100$ mg L^{-1} Type of iron in range Auxiliary energy in range	Given in Fig. 8a and b	
Using the mixture D-optimal desing[a]			
X_{colour}, X_{TOC} (US) $\Rightarrow$ maximum X_{colour}, X_{TOC} (UV-A) $\Rightarrow$ maximum	$0.95 < [Fe^{2+}\ (mol\,L^{-1})] \times 10^3 < 1.05$ $0.02 < [H_2O_2\ (mol\,L^{-1})] < 0.06$ $[LAS] = 0.30 \times 10^{-3}$ mol L^{-1}	$[Fe^{2+}] = 0.97 \times 10^{-3}$ mol L^{-1} $[H_2O_2] = 0.03$ mol L^{-1}	60.1%

[a] Single point optimization was obtained for both auxiliary energy used (US and UV-A).

concentration in the system (Table 6, Figs. 4 and 7). Performed study showed the positive influence of the increasing LAS content in the system with the simultaneous negative influence of the H_2O_2 (Fig. 5). Effects of the LAS in the treated system will be discussed in the following subsections.

Optimization performed using the BBD models, according to the DFA methodology resulted in the optimal regions, where all studied parameters could be varied moderately (Fig. 6). In order to obtain single optimal point, D-optimal mixture design was used. The rationale for the implementation of the mixture design can be comprehended when observing the influencing factors as components of a mixture. In other words, the proportions of each factor/parameter are more interesting to observe than the total amounts. Having in mind that the results of DFA (Fig. 6) cover a certain area with the high desirability ($d \geq 0.7$), the optimal formulation of reagents (Fe^{2+} and H_2O_2) and LAS within this area is possible to find only if studying the proportions. Implementation of the mixture design after optimization based on the BBD models, gave the more narrow area whereas decolourization and mineralization extents depend on the mixture composition, i.e. proportion of each observed compound of the mixture (Fe^{2+}, H_2O_2 and LAS) (Fig. 7, Table 6). Mixture models obtained in this work (Table 6) correspond to the most common quadratic or modified cubic Scheffé models, Eqs. (7a) and (7b) [17]

$$E(X) = \sum_i \beta_i x_i + \sum \sum_{i<j} \beta_{ij} x_i x_j \quad (7a)$$

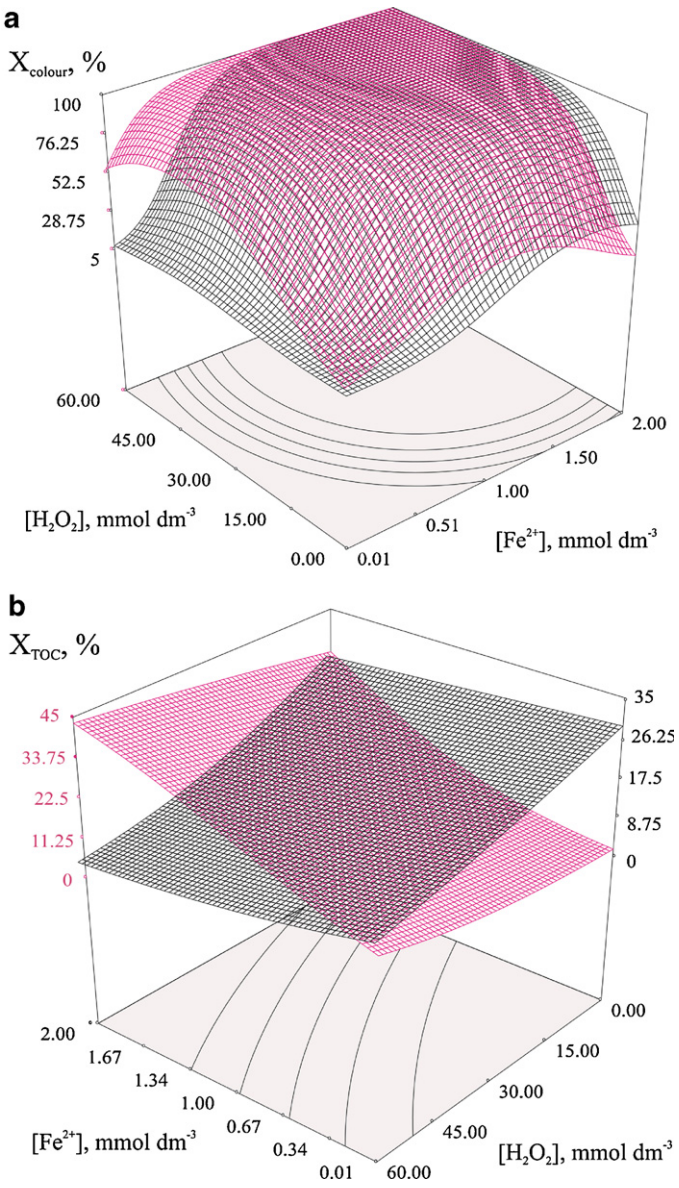

Fig. 4. Simulation of the average (a) decolourization and (b) mineralization yields achieved by US/UV-A Fenton process (RV2+LAS solution) as a function of the process parameters; no LAS in the solution (black grid) and 100 mg L^{-1} of LAS (pink grid). (For interpretation of the references to color in this figure legend, the reader is referred to the web version of the article.)

$$E(X) = \sum_i \beta_i x_i + \sum \sum_{i<j} \beta_{ij} x_i x_j + \sum \sum_{i<j} \delta_{ij} x_i x_j (x_i - x_j) + \sum \sum \sum_{i<j<k} x_i x_j x_k \quad (7b)$$

where the $\Sigma \beta_i x_x$ term is called the linear blending term, and the quadratic and cubic terms should not be thought of as interaction but instead are called non-linear blending terms. If β_{ij} is positive, the term is synergistic, while if it is negative it is called antagonistic. δ_{ij} symbolizes the differences.

BBD technique is widely used due to its reliability. However it is common to obtain wide optimal area upon optimization via DFA. On the other hand, mixture design cannot be easily applied to study the process parameters in the wide range as it can be done by using BBD. Narrow range of process parameters can be translated into the

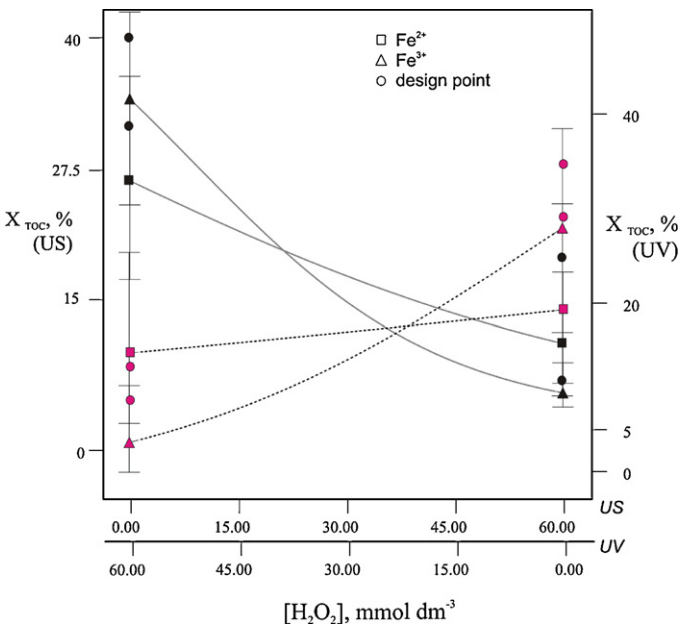

Fig. 5. Dependency of the mineralization yield on the H_2O_2 concentration in RV2+LAS solution due to the implementation of the US (black marker – solid line) and UV irradiation (pink marker – dashed line). (For interpretation of the references to color in this figure legend, the reader is referred to the web version of the article.)

mixture constraints giving the unbiased results, especially after the numerical optimization. It is quite common to get a single optimal composition when using mixture design. Utilizing of the BBD as a base for the further simulations and mixture design advantages, a single optimal point was found through this *two-step* optimization (Table 7). Results of the BBD analysis allowed also the interpretation of LAS pseudo-catalytic effect.

3.2. Degradation kinetics

As it can be seen from Fig. 8a and b, two distinct regions can be depicted while observing the mineralization kinetics. In the case of simulated dye bath effluent treated in 10-fold dilution (WW 1:10) first kinetic region can be determined in the first 10 min of the applied processes (Fig. 8a), while in the case of the concentrated effluent (WW), first kinetic region was observed in the shortened time interval, i.e. first 7 min of the processes (Fig. 8b). Fast mineralization, referred to the both US/Fe^{2+}/H_2O_2 and UV-A/Fe^{2+}/H_2O_2 process, was observed in the first kinetic region (Fig. 9a). As shown at the Fig. 8a, experimental data better fits the exponential law, implying on the fact that a mineralization observed in the first 7–10 min follows pseudo-first-order kinetics (Fig. 9a). Referred to the treatment of the WW 1:10, estimated first-order rate constants were, 0.0478 min^{-1} and 0.0509 min^{-1} for US/Fe^{2+}/H_2O_2 and UV-A/Fe^{2+}/H_2O_2 process, respectively. In the case of the treatment of WW, observed constants were 0.0753 min^{-1} for US/Fe^{2+}/H_2O_2 and 0.0730 min^{-1} for UV-A/Fe^{2+}/H_2O_2 process.

This obvious difference in the observed rates depending on the dilution of the effluent imply on the significant difference in the oxidative species generation in this two cases. If mineralization process is simply observed as shown by Eq. (8), organic compounds

$$\text{Organic compounds (OC)} + OH^{\bullet} \rightarrow CO_2 + H_2O + \text{other mineralization products} \quad (8)$$

then the explanation for the faster mineralization arose from the fact that in "concentrated" system more hydroxyl radicals should be generated. This is actually supported by the fact that many of the

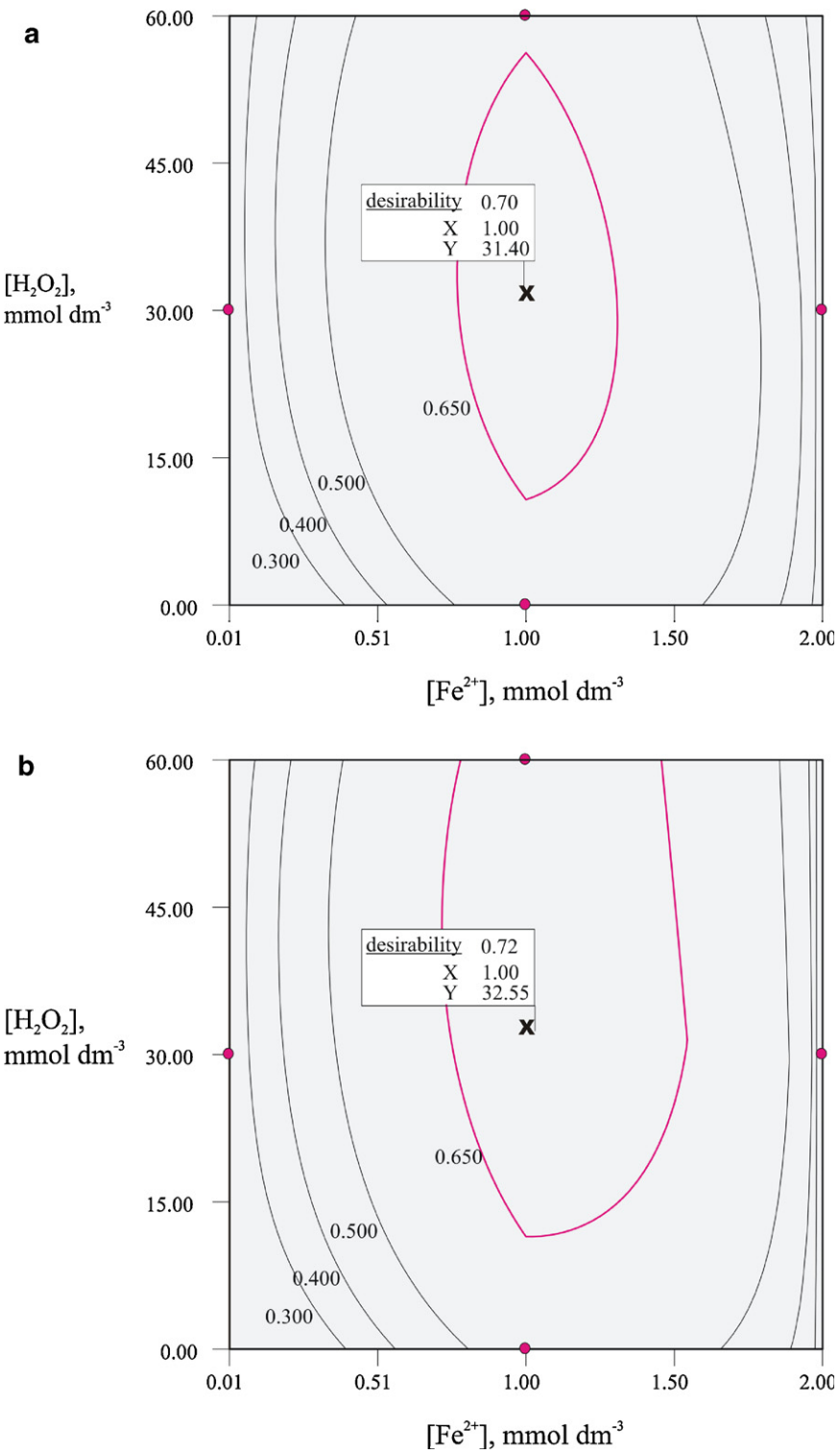

Fig. 6. Result of numerical optimization according to DFA – contour plots for optimal design space for the (a) US/Fe^{2+}/H_2O_2 and (b) UV-A/Fe^{2+}/H_2O_2 process according to BBD (100 mg L^{-1} of LAS in RV2+LAS solution).

species in the dye bath effluent (Na, LAS, compounds with the alkyl chains) promote the Fenton reaction [21–23]. Dihydroxybenzenes could also act as promoters for the self-catalyzed Fenton [24]. As the "head" of the used surfactant is the substituted benzene ring, it presents a potential for the hydroxylation during the applied process and consequently a large source of the Fenton promoters. On the other hand, a "tail" of the used surfactant, i.e. long alkyl chain, could give [$-CH_2-$ $-^{\bullet}CH-$] radicals that have an evident role in the radical transfer mechanisms [25]. Therefore, the following scheme should allow a better interpretation of the ongoing process (Eq. (9)).

$$OC \xrightarrow[\text{oxidative species \& promoters}]{OX} \text{mineralization products} \quad (9)$$

As implied by the scheme given in Eq. (9), presence and concentration of OX, i.e. all oxidative species ($OH^{\bullet}$, $SO_4^{\bullet-}$, $O_2^{\bullet-}$, etc.) and promoters influence the observed mineralization rate constants.

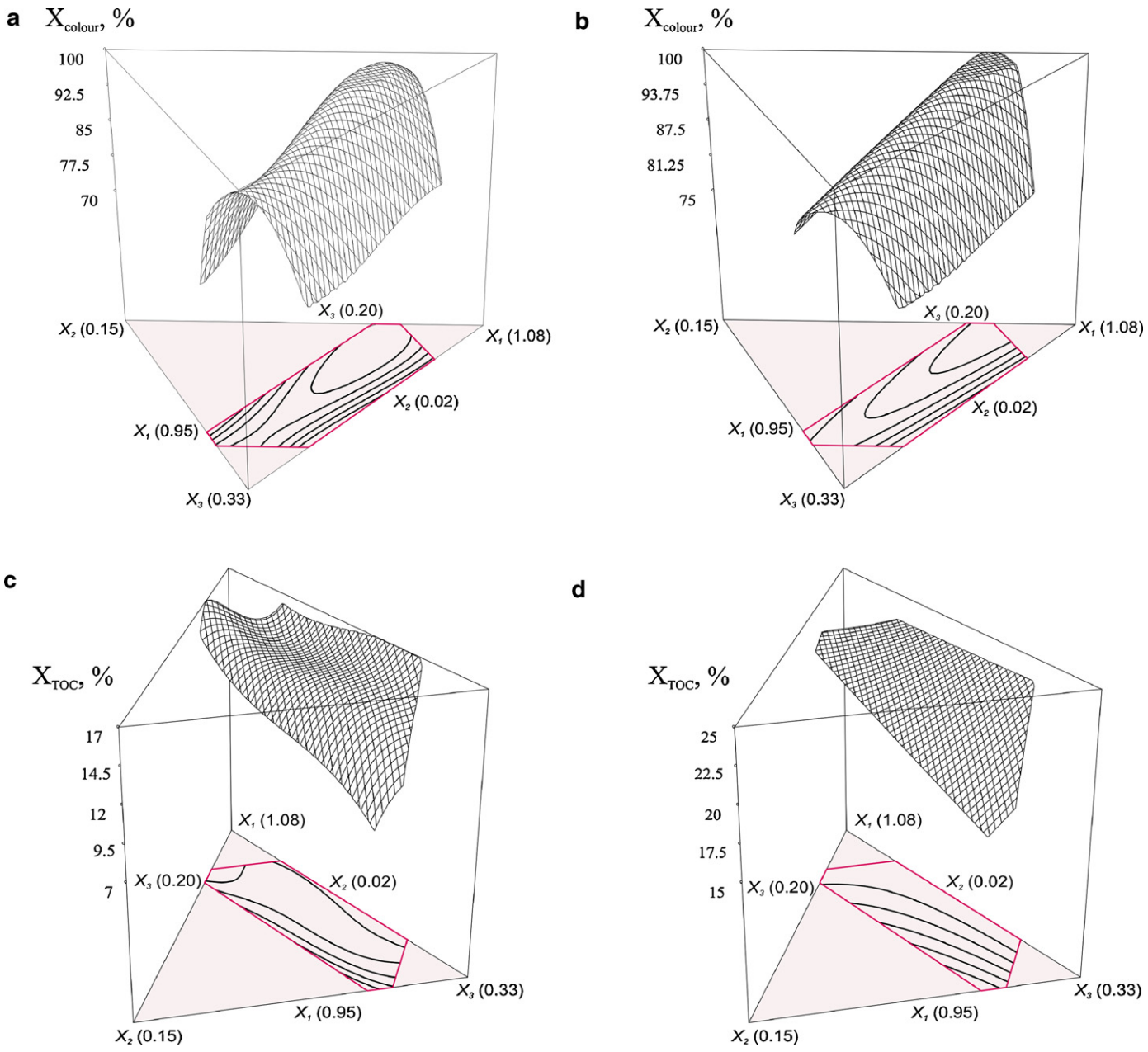

Fig. 7. Dependency of the simulated decolourization and mineralization yields on the mixture composition in the (a) and (c) US and (b) and (d) UV-A assisted Fenton process.

In the second kinetic region, from tenth or seventh minute up to the 60 min, slow mineralization has been observed. Mineralization kinetics in this region could be described by the zeroth order kinetics (Fig. 9b). Observed rate constants are more or less the same, ranging from 9×10^{-4} to 2.1×10^{-3} min^{-1} (assuming normalized TOC values) with no significant difference in the overall rate due to the dilution in the treated sample (Fig. 9b). Mineralization extents achieved in the second kinetic region depend only on the characteristics, i.e. parameters of the applied process. Therefore, optimization performed in the frame of this work played an important role in finding of the conditions that would allow the highest extents of the organic pollutant degradation.

3.3. Highlights of the study

The presented study contributed to the better understanding of the processes occurring in the system. LAS molecules exhibit the pseudo-catalytic behavior in the studied systems, and it was from the utmost importance to study this effect separately. Results of the experimental design proved the idea of LAS pseudo-catalytic effect and gave the solid base for further discussion. It is worth to notice that the LAS amount in model solution (RV2+LAS) set as an optimization criterion (Table 7) represents the same amount of LAS in WW 1:10. From the environmental point of view, it is important to define the conditions necessary for the treatment of WW 1:10 and the corresponding kinetics, since WW 1:10 is the quite good representation of real textile wastewater [13]. On the other hand, kinetic study of WW contributes to the knowledge related to the influence of the auxiliary chemicals on the performance of advanced oxidation processes.

As it is widely accepted fact, dye molecule can be readily degraded following the mechanism of the advanced oxidation by hydroxyl radicals. In the both applied processes, US/Fe^{2+}/H_2O_2 and UV-A/Fe^{2+}/H_2O_2, mechanism of the dye molecule degradation follows the same pattern. On the other hand, it is considered that a long chain of the surfactant molecule can be oxidized by a pyrolysis

Table 8
Mineralization yields achieved after 30 min of treatment of LAS model solution by ultrasonic assisted processes (model solution prepared by dissolving only 100 mg of Na-dodecylbenzene sulfonate in 1L of distilled water).

Applied process	X_{TOC}, %
US/Fe^{2+}	6.54
US/H_2O_2	4.88
US/Fe^{2+}/H_2O_2	**15.75**
US	6.43

within the bubble formed during the cavitation. That phenomena should results with an enhancement of the overall mineralization rate achieved by the US assisted Fenton process. LAS and H_2O_2 compete for the cavitation reaction sites, as it can be concluded from Fig. 5 and Table 8, which presents a positive aspect for the treatment of the wastewaters containing surfactants, since a minor amount of H_2O_2 is needed. As it has been already provided, there is a negligible difference in the mineralization kinetics observed for the US and UV-A assisted Fenton oxidation in the case of both model RV2 wastewater and simulated dyebath effluent treated in dilution and without dilution (Fig. 10a and b). One possible explanation is the low performance of the equipment used for the sonication. Especially due to the fact that the yield of the [–CH_2 – •CH–] radicals (or –•CH–), responsible for the propagation of the ongoing reactions, depends only on the frequency and it is independent of the amplitude of the ultrasound [25]. High power of the ultrasound evident by the visual observation of the cavitation and the pronounced thermal effects is therefore insufficient for the full contribution to the mineralization if working at a single frequency.

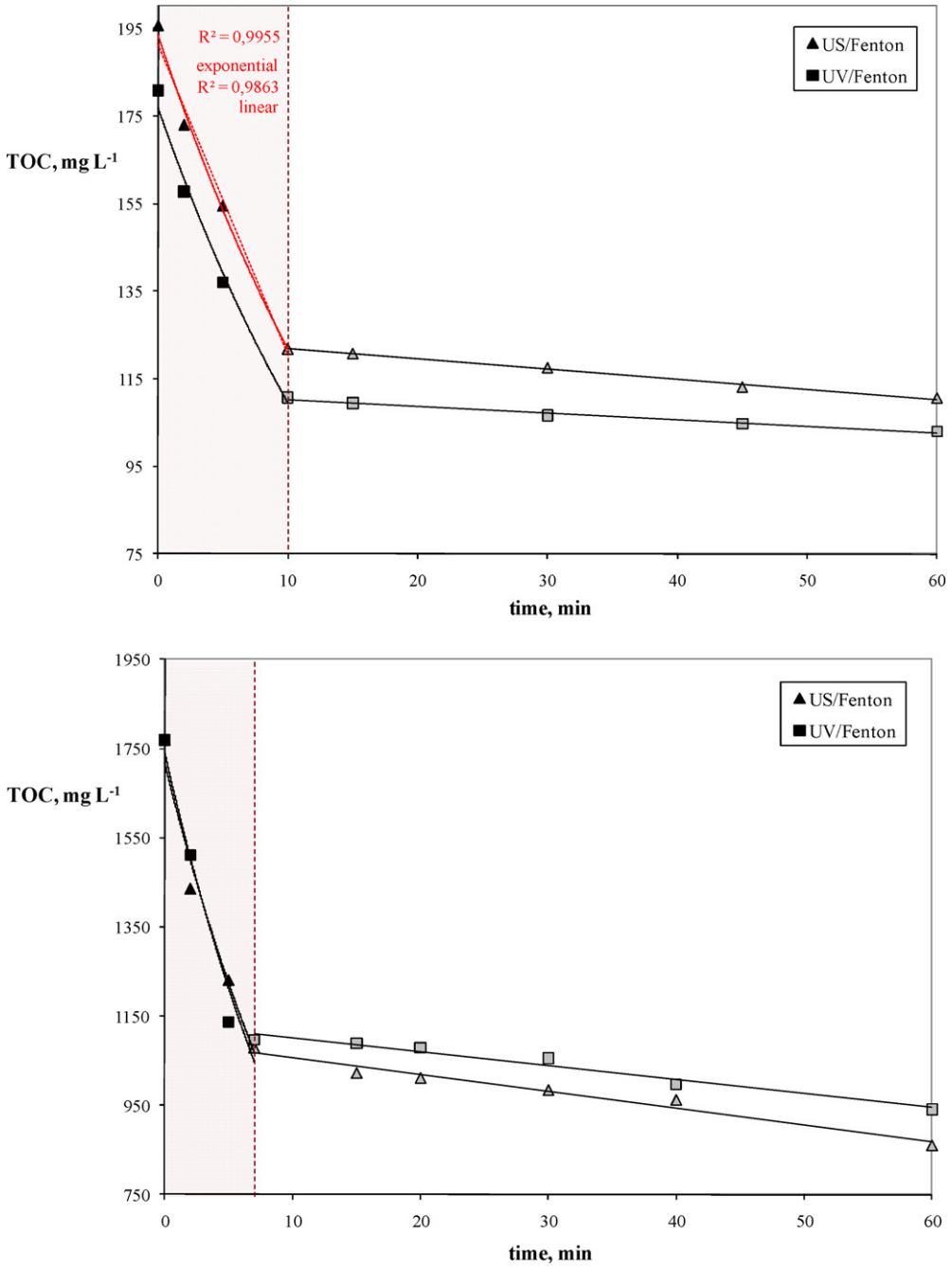

Fig. 8. Kinetics of the US and UV-A assisted Fenton oxidation of the simulated dyestuff effluent; (a) WW 1:10, (b) WW at established optimal conditions (see Table 7).

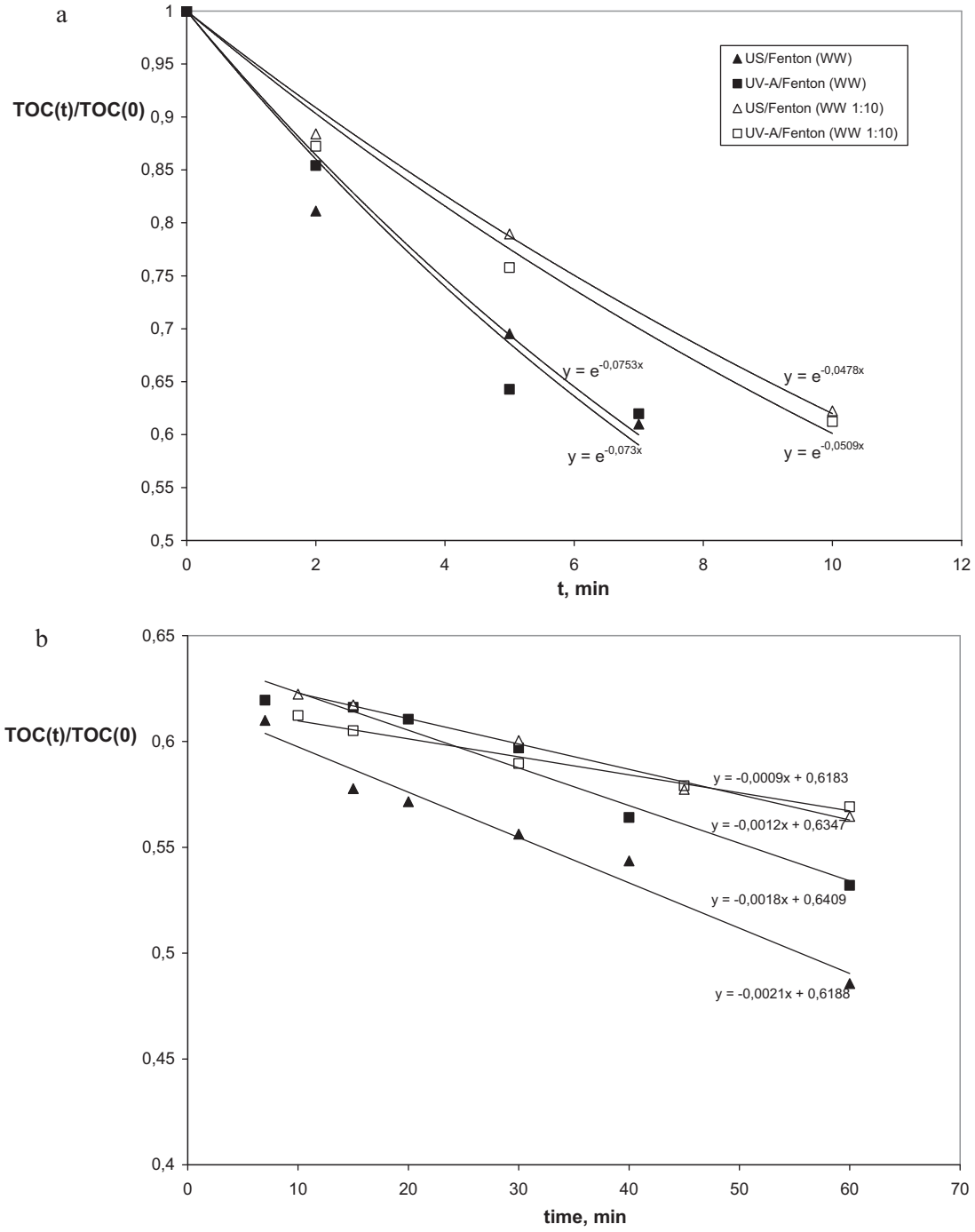

Fig. 9. Kinetics of the US and UV-A assisted Fenton oxidation of the simulated dyestuff effluent, (a) first kinetic region – fast kinetics, (b) second kinetic region – slow kinetics.

Another explanation for the apparent equal mineralization efficiency obtained by the US and UV-A assisted Fenton (Fig. 10a) is the possibility of the regeneration of Fe^{2+} from the organic complexes formed during the oxidation cycle using the UV irradiation, Eq. (6). The degradation of the molecules initially present in the system; dye, surfactant and other organics, is rather fast and the smaller molecules that acts as chelating agents for Fe^{3+} are readily formed [26]. Assuming the simultaneous constant increase in the Fe^{3+} concentration in the system [6], complex Fe^{3+}–OC species are formed and the iron is being "trapped". Implementation of UV light to such system allows the breakage of complexes and the release of Fe^{2+} necessary for the Fenton cycle. It can be concluded that the US and UV-A application on the Fenton oxidation have the apparent equal effect on the overall efficiency, yet different mechanisms were observed. US contributes due to the oxidation of particular compound in the cavitation bubbles and at the interphase giving the variety of promoting radicals, while by the implementation of UV irradiation the formation of undesired products (Fe^{3+}–OC) can be avoided and Fe^{2+} can be easily regenerated. It is obvious in the case of the treatment of the model RV2 wastewater containing 100 mg L^{-1} of LAS (Fig. 10b). In the case of US assisted Fenton oxidation a rapid mineralization was depicted in the beginning of the process, while in the case of UV-A assisted Fenton a constant mineralization has been observed. Initially rapid mineralization indeed suggests the fast degradation of LAS by US related phenomena, while the slower mineralization after the

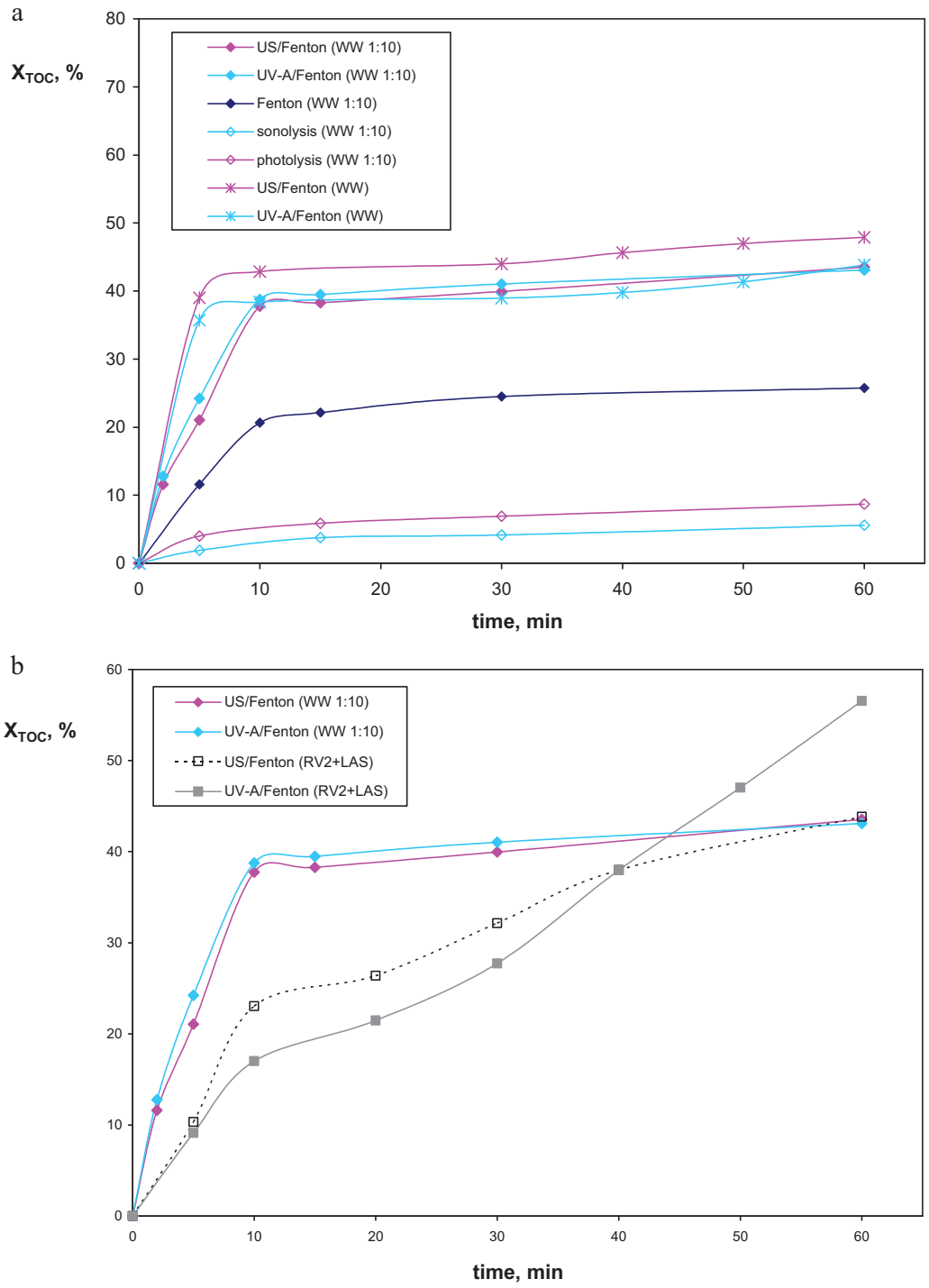

Fig. 10. Comparison of the applied processes on the (a) simulated dyehouse effluent (WW and WW1:10), and (b) WW 1:10 and RV2+LAS model solution.

first 10 min suggests an entrance into the termination cycle of a radical chain. The constant mineralization observed during the UV-A/Fe^{2+}/H_2O_2 process confirmed the simultaneous degradation of model pollutants (dye – RV2 and LAS) towards smaller molecules and regeneration of Fe^{2+} by breaking down the Fe^{3+}–OC complexes.

The presence of the surfactant in the amounts higher than 25% (w/w) compared to the initial dye concentration resulted in a significant decrease of the decolourization achieved in the first 15 min of the process, suggesting the competitiveness for the •OH radicals. In the case of US/Fe^{2+}/H_2O_2 higher amounts of surfactant means the aggregation of its molecules on the cavity surface trapping the •OH radicals responsible for the initial breakage of the dye molecule, i.e. azo bond cleavage [26]. In the case of UV-A/Fe^{2+}/H_2O_2 process performed in the well-mixed system, surfactant and dye molecules are equally present in the bulk having the same opportunities for the hydroxyl attack. As the amount of surfactant molecules increases, the competitiveness for the •OH radicals is observed.

4. Conclusions

The treatment possibilities for the simulated dyehouse wastewater by the Fenton oxidation US and UV-A assisted were explored.

Simulated dyehouse wastewater consisted of the reactive azo dye, C.I. Reactive Violet 2 (RV2), surfactant (LAS) and other additional compounds. The influence of LAS has been evaluated through the statistical models according to the study of the selected processes in the model wastewater containing only RV2 and different amounts of LAS. The observed positive influence of LAS on the overall efficiency assumed the decrease in the demand for the oxidant, i.e. H_2O_2.

Both US and UV-A implementation significantly contributed to the overall mineralization. E.g., only 26% of mineralization was achieved by only Fenton process applied for the treatment of the dyehouse effluent in 10-fold dilution, while 43% of mineralization was achieved by using US or UV-A assisted Fenton after the 60 min. US contributes due to the oxidation of particular compound – surfactant in the cavitation bubbles and at the interphase giving the variety of promoting radicals, –•CH–. Degradation of primary pollutants in the system is rather fast, leading to the formation of smaller organic molecules, CO_2 and H_2O. Among by-products, there are molecules that act as chelating agents for Fe^{3+} formed during Fenton cycle. By the implementation of UV irradiation the formation of undesired products (Fe^{3+}–OC) can be avoided and Fe^{2+} can be easily regenerated by breaking down the Fe^{3+}–OC complexes.

The single optimal point was established for US/Fe^{2+}/H_2O_2 and UV-A/Fe^{2+}/H_2O_2 processes through the *two-step* optimization. The further advantage of this approach refers to the possibility of the integration of these two processes in the future studies.

Acknowledgments

Purchase of equipment used in this work was financially supported by The National Foundation for Science, Higher Education and Technological Development of the Republic of Croatia, in the frame of the Project #04/14, *Wastewater Treatment in DINA-Petrokemija Omišalj as a Contribution to Ecosystem Preservation*. We would also like to acknowledge the financial support from the Croatian Ministry of Science, Education and Sport, Project #125-1253092-1981.

References

[1] M.S. Secula, G.D. Suditu, I. Poulios, C. Cojocaru, I. Cretescu, Response surface optimization of the photocatalytic decolorization of a simulated dyestuff effluent, Chem. Eng. J. 141 (2008) 18–26.
[2] I. Grčić, D. Vujević, J. Šepčić, N. Koprivanac, Minimization of organic content in simulated industrial wastewater by Fenton type processes: a case study, J. Hazard. Mater. 170 (2009) 954–961.
[3] L. Núñez, J.A. Garcia-Hortal, F. Torrades, Study of kinetic parameters related to the decolourization and mineralization of reactive dyes from textile dyeing using Fenton and photo-Fenton processes, Dyes Pigments 75 (2007) 647–652.
[4] J.M. Chacon, M.T. Leal, M. Sanchez, E.R. Bandala, Solar photocatalytic degradation of azo-dyes by photo-Fenton process, Dyes Pigments 69 (2006) 144–150.
[5] D.H. Bremner, R. Molina, F. Martinez, J.A. Melero, Y. Segura, Degradation of phenolic aqueous solutions by high frequency sono-Fenton systems (US-Fe_2O_3/SBA-15-H_2O_2), Appl. Catal. B 90 (2009) 380–388.
[6] I. Grčić, M. Obradović, D. Vujević, N. Koprivanac, Sono-Fenton oxidation of formic acid/formate ions in an aqueous solution: from an experimental design to the mechanistic modeling, Chem. Eng. J. 164 (2010) 196–207.
[7] X. Liu, F. Wu, N. Deng, Photoproduction of hydroxyl radicals in aqueous solution with algae under high-pressure mercury lamp, Environ. Sci. Technol. 38 (2004) 296–299.
[8] J.A. Frim, J.F. Rathman, L.K. Weavers, Sonochemical destruction of free and metal-binding ethylenediaminetetraacetic acid, Water Res. 37 (2003) 3155–3163.
[9] P. Chowdhury, T. Viraraghavan, Sonochemical degradation of chlorinated organic compounds, phenolic compounds and organic dyes – a review, Sci. Total Environ. 407 (2009) 2474–2492.
[10] B. Yim, Y. Yoo, Y. Maeda, Sonolysis of alkylphenols in aqueous solution with Fe(II) and Fe(III), Chemosphere 50 (2003) 1015–1023.
[11] L. Yang, J.F. Rathman, L.K. Weavers, Sonochemical degradation of alkylbenzene sulfonate surfactants in aqueous mixtures, J. Phys. Chem. B 110 (2006) 18385–18391.
[12] D. Drijvers, H. van Langenhove, L. Nguyen Thi Kim, L. Bray, Sonolysis of an aqueous mixture of trichloroethylene and chlorobenzene, Ultrason. Sonochem. 6 (1999) 115–121.
[13] I.A. Alaton, I.A. Balcioglu, D.W. Bahnemann, Advanced oxidation of a reactive dyebath effluent: comparison of O_3, H_2O_2/UV-C and TiO_2/UV-A processes, Water Res. 36 (2002) 1143–1154.
[14] I. Grčić, N. Koprivanac, D. Vujević, S. Papić, Removal of atrazine from simulated groundwater by AOTs, J. Adv. Oxid. Technol. 11 (2008) 91–96.
[15] S. Ray, RSM: a statistical tool for process optimization, Ind. Tex. J. 117 (2006) 24–30.
[16] S. Bae, M. Shoda, Statistical optimization of culture conditions for bacterial cellulose production using Box–Behnken design, Biotechnol. Bioeng. 90 (2005) 20–28.
[17] J.A. Cornell, Experiments and mixtures, in: Designs Models and the Analysis of Mixture Data, 2nd ed., J. Wiley and Sons, New York, 1990.
[18] L. Eriksson, E. Johansson, C. Wikström, Mixture design—design generation, PLS analysis, and model usage, Chemometr. Intell. Lab. Syst. 43 (1998) 1–24.
[19] A. Mannarswamy, S.H. Munson-McGee, P.K. Andersen, D-optimal designs for the cross viscosity model applied to guar gum mixtures, J. Food Eng. 97 (2010) 403–409.
[20] P. Mura, S. Furlanetto, M. Cirri, F. Maestrelli, A.M. Marras, S. Pinzauti, Optimization of glibenclamide tablet composition through the combined use of differential scanning calorimetry and D-optimal mixture experimental design, J. Pharmaceut. Biomed. 37 (2005) 65–71.
[21] J.M. Joseph, H. Destaillats, H.-M. Hung, M.R. Hoffmann, The sonochemical degradation of azobenzene and related azo dyes: rate enhancements via Fenton's reactions, J. Phys. Chem. A 104 (2000) 301–307.
[22] M.A. Tarr, Fenton and modified Fenton methods for pollutant degradation, in: Chemical Degradation Methods for Wastes and Pollutants – Environmental and Industrial Applications, Marcel Dekker, Inc, New York, 2003, pp. 165–200.
[23] L. Becker, J.L. Bada, K. Kemper, K.S. Suslick, The sonoluminescence spectrum of seawater, Mar. Chem. 40 (1992) 315–320.
[24] D. Contreras, J. Rodriguez, J. Freer, B. Schwederski, W. Kaim, Enhanced hydroxyl radical production by dihydroxybenzene-driven Fenton reactions: implications for wood biodegradation, J. Biol. Inorg. Chem. 12 (2007) 1055–1061.
[25] J.Z. Sostaric, A comparative sonochemical reaction that is independent of the intensity of ultrasound and the geometry of the exposure apparatus, Ultrason. Sonochem. 15 (2008) 1043–1048.
[26] I. Grčić, D. Vujević, N. Koprivanac, Modeling the mineralization and discoloration in colored systems by (US)Fe^{2+}/H_2O_2/$S_2O_8^{2-}$ processes; a proposed degradation pathway, Chem. Eng. J. 157 (2010) 35–44.